

## Dark-dark solitons and modulational instability in miscible two-component Bose-Einstein condensates

M. A. Hofer, <sup>1,\*</sup> J. J. Chang, <sup>2</sup> C. Hamner, <sup>2</sup> and P. Engels <sup>2</sup>

<sup>1</sup>North Carolina State University, Department of Mathematics, Raleigh, North Carolina 27695, USA

<sup>2</sup>Washington State University, Department of Physics and Astronomy, Pullman, Washington 99164, USA

(Received 19 May 2010; revised manuscript received 3 March 2011; published 14 October 2011)

We investigate the dynamics of two miscible superfluids experiencing fast counterflow in a narrow channel. The superfluids are formed by two distinguishable components of a trapped dilute-gas Bose-Einstein condensate (BEC). The onset of counterflow-induced modulational instability throughout the cloud is observed and shown to lead to the proliferation of dark-dark vector solitons. These solitons do not exist in single-component systems, exhibit intriguing beating dynamics, and can experience a transverse instability leading to vortex line structures. Experimental results and multidimensional numerical simulations are presented.

DOI: [10.1103/PhysRevA.84.041605](https://doi.org/10.1103/PhysRevA.84.041605)

PACS number(s): 67.85.De, 03.75.Kk, 03.75.Lm, 05.45.Yv

Superfluids are a robust model system for the investigation of nonlinear fluid flow. Governed by an underlying macroscopic wave function, superfluids can display a large variety of nonlinear wave phenomena in the context of matter waves. In Bose-Einstein condensates (BECs), nonlinear structures including solitons, vortices, and vortex rings have been the focus of intense research efforts [1,2]. In this Rapid Communication, we investigate the regime of fast counterflow between two distinguishable superfluids in a narrow channel and observe dynamics leading to unique structures. Modulational instability (MI), in which small perturbations to a carrier wave, reinforced by nonlinearity, experience rapid growth [3], plays a key role in the dynamics. In many nonlinear systems, MI leads to the breakup of periodic wave trains, as in sufficiently deep water [4], as well as the formation of localized structures in optics [5] and BECs [6]. In our case, MI-induced regular density modulations, formed throughout the BEC, lead to the emergence of a large number of *beating dark-dark* solitons. These solitons—which exhibit periodic energy exchange between the two condensate components [7]—are a generalization of static dark-dark solitons [8]. They are distinctly different from all previously observed solitons in BECs, including dark-bright solitons which were generated in a two-component mixture by marginally critical counterflow-induced MI near a density edge [9]. We perform three-dimensional (3D) numerical simulations to corroborate this interpretation and furthermore identify a subsequent transverse instability resulting in multidimensional structures such as vortex lines (see Ref. [10] for the scalar counterpart).

We study superfluid counterflow with an experimental system consisting of BECs with typically  $8 \times 10^5$  atoms of  $^{87}\text{Rb}$ . The BECs are confined in a cigar-shaped, far-detuned optical dipole trap with measured trap frequencies of  $2\pi \times \{1.5, 140, 178\}$  Hz with a horizontal weakly confined axis. By starting with all atoms in the  $|F, m_F\rangle = |1, -1\rangle$  hyperfine state and transferring  $\sim 50\%$  of the atoms to the  $|2, -2\rangle$  state via a 1-ms-long microwave sweep, a perfectly overlapped two-component mixture is created. The predicted scattering lengths for these states [11] imply that this mixture is miscible [12], which is also supported by our experimental observation

of no phase separation for an unperturbed mixture of these states. To induce relative motion between the components, an external magnetic gradient is applied along the elongated (axial) direction. The gradient pulls atoms in the  $|2, -2\rangle$  state to the left and those in the  $|1, -1\rangle$  state to the right. The atoms are imaged using a free-expansion imaging procedure. Each experimental image shows an upper cloud consisting of the  $|2, -2\rangle$  atoms after 7 ms of free expansion and a lower cloud consisting of the  $|1, -1\rangle$  atoms after 8 ms of free expansion. Both clouds are imaged during the same experimental run.

Experimental data showcasing the formation of a very dense counterflow-induced MI pattern are presented in Fig. 1. In the presence of a 10.4 mG/cm axial gradient, a gradual pattern formation starts after 70 ms of smooth evolution [Figs. 1(a) and 1(b)]. We first observe pattern formation in noncentral regions where the two condensates have differing densities [Fig. 1(b)]. This is due to the dependence of the critical velocities for counterflow-induced MI on the two-component density ratio being largest when the densities are equal [9,13]. After  $\sim 25$  ms, a very dense and regular MI pattern fully develops, filling the entire BEC [Fig. 1(c)]. The modulations in the two components are offset in the axial direction in a staggered way such that one component fills the depressions in the other. Under the continued influence of the axial gradient, the regular pattern of Fig. 1(c) quickly becomes uneven and irregular. Alternatively, if the gradient is switched off after the MI pattern has fully developed, we frequently observe the formation of black dots such as those marked by the arrows in Fig. 1(d), which might indicate the generation of vorticity. We note recent theoretical work suggesting that counterflow-induced MI may be used to generate quantum turbulence [14].

Imparting slow counterflow conditions, implying a slow MI onset in the quasiuniform background, we previously generated a dark-bright soliton train emanating *locally* from a density edge [9]. In contrast, the fast counterflow considered here leads to a rapid MI onset and pattern formation *throughout* the condensates.

MI theory agrees quantitatively with the experimentally observed patterns as we now explain (Fig. 2). For a uniform counterflow, the onset of MI corresponds to a complex sound speed (see Ref. [15]) and exhibits a preferred wave number  $k_{\text{max}}$  corresponding to the maximum growth rate

\*mahoefer@ncsu.edu

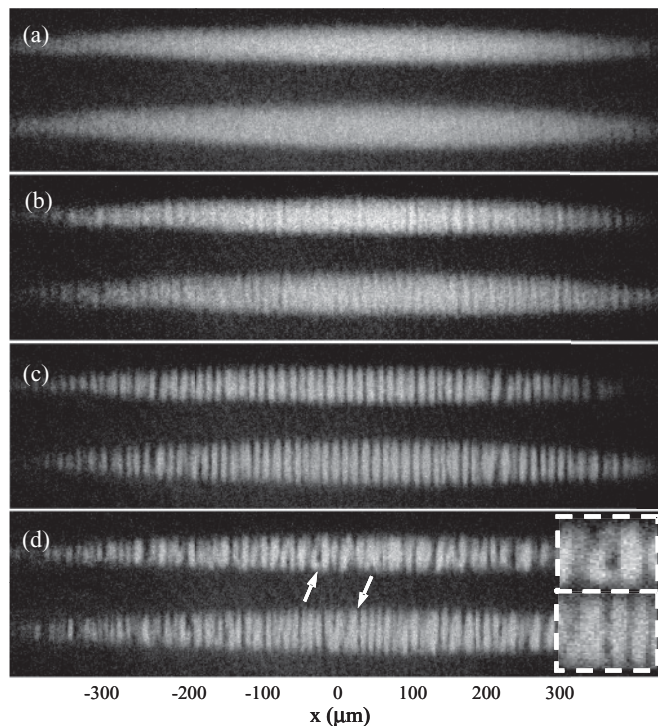


FIG. 1. Counterflow-induced MI in the presence of a strong magnetic gradient of 10.4 mG/cm. Evolution times (a) 10 ms, (b) 70 ms, and (c) 95 ms. (d) After MI onset, the axial gradient is turned off, followed by a trapped evolution time of 20 ms.

$g_{\max}$ , both depending on the counterflow speed. Unfortunately, our imaging procedure does not allow us to determine the counterflow speeds experimentally. However, we can take two independent theoretical approaches, described below, to extract the onset velocities from our experimental data. The fact that these two independent approaches lead to consistent results gives quantitative credence to the theory. First, we use the analytical theory in Refs. [9] and [13] to calculate the counterflow speed  $v_{\text{fit}}$  whose corresponding  $k_{\max}$  equals the experimentally observed pattern periodicity at the trap center where the densities are assumed to be equal (the solid, black curve in Fig. 2). In a second, independent approach, we assume spatially uniform counterflow whereby the applied gradient leads to unimpeded acceleration of each

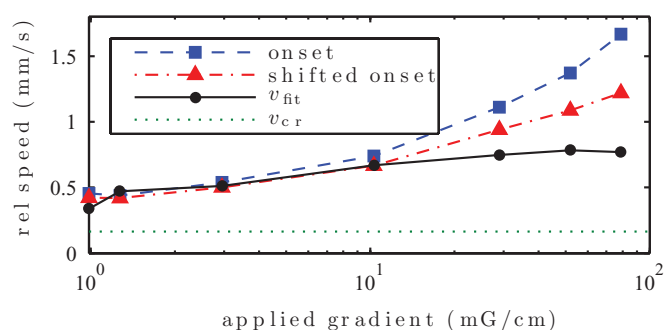


FIG. 2. (Color online) Consistent predictions of counterflow speed based on wavelength and onset time measurements of MI as a function of applied gradient. For details see the text.

component (calculated from the atomic magnetic moment and the magnitude of the applied gradient). Using this simple model, experimentally determined onset times for MI are converted to relative speeds at the onset of the MI pattern (the dashed blue curve in Fig. 2). The dashed-dotted red curve in Fig. 2 uses the same uniform counterflow model but shifts the measured MI onset time by  $-1/g_{\max}$ . Subtracting this time accounts for the development of the instability and leads to a better approximation of the true relative speed that sets the pattern periodicity. The resulting curve interpolates the two models. The lowest dotted curve is the predicted critical speed in the condensate center ( $v_{\text{cr}} = 0.16$  mm/s) demonstrating fast counterflow [16]. Despite the approximations made, the curves exhibit agreement for small-to-moderate gradients, suggesting that the observed dynamics are theoretically described by counterflow-induced MI. Discrepancies at large gradients are likely due to the large accelerations involved and spatial nonuniformity.

We now investigate the dynamics of the MI onset by using a smaller gradient of 1.4 mG/cm so that  $k_{\max}$  is reduced relative to Fig. 1, enabling better experimental observation of individual features (Fig. 3). After smooth counterflow, MI

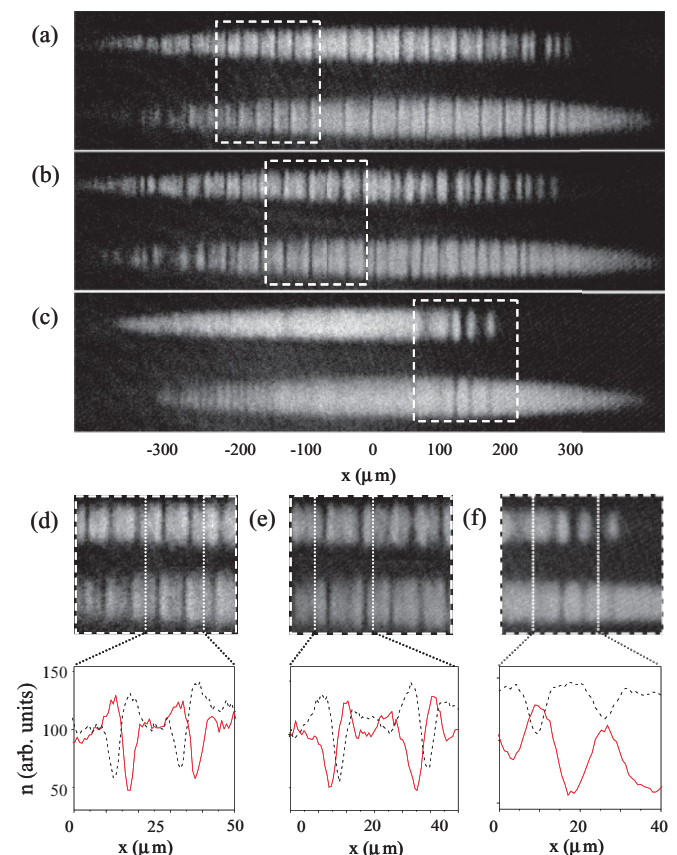


FIG. 3. (Color online) (a), (b) Dark-dark solitons as a result of MI after applying a gradient of 1.4 mG/cm for 350 and 380 ms, respectively. (c) Formation of dark-bright solitons when a small magnetic gradient of 0.2 mG/cm is applied. The gradient is left on for 1000 ms before the start of the expansion sequence. (d)–(f) Enlargement of boxed region in (a)–(c), respectively. The red solid lines are integrated cross sections of the  $|2, -2\rangle$  state, and the black dashed lines of the  $|1, -1\rangle$  state.

sets in across the BEC, leading to a regular array of dark-dark solitons [Figs. 3(a), 3(b), 3(d), and 3(e)]. In accordance with theory and our numerics (see below), the dark-dark solitons exhibit a dynamic beating, as seen by comparing the integrated cross sections of Figs. 3(d) and 3(e), noting the order of the notch and bump feature in each component. While our destructive imaging technique does not allow us to determine the exact beat frequency, our 3D numerics indicate a time scale of 15 ms per period [15]. The dark-dark solitons we observe here are unique and distinct from the dark-bright solitons that have been observed previously in BECs [9,17,18], which are distinguished by their far-field conditions and dynamics. To facilitate a comparison, an example dark-bright soliton train, seeded at the condensate interfaces and generated by slow, marginally critical counterflow [9], is shown in Figs. 3(c) and 3(f). A dark-bright soliton consists of a dark notch in one component, filled by a localized density bump of the second component. In contrast, the beating dark-dark soliton asymptotes to nonzero densities in both components and dynamically changes its shape, with each component possessing a density bump adjacent to a notch which alternate their relative positions in time (see also Fig. 6 below).

The dynamics are well reproduced by 3D numerical simulations [15] of the vector, mean-field Gross-Pitaevskii equation with initial conditions and parameters corresponding to the experiments in Figs. 1(a)–1(c) and 3(a) and 3(b) [19]. As with experiment, a smooth, accelerating counterflow develops due to the axial field gradient. Dark-bright solitons form at the edges of the condensates until the rapid growth of large-scale modulations is observed [Figs. 4(a) and 4(b)]. For moderate gradients in Figs. 4(a), 4(c), and 4(e), these modulations rapidly develop into a number of localized, essentially one-dimensional (1D) beating dark-dark solitons with an initial approximate spacing  $2\pi/k_{\max}$ . Continued evolution results in interactions and eventual solitary wave transverse breakup at approximately  $t = 600$  ms.

For the strong gradient case, our numerics show the development of axial modulations by approximately  $t = 125$  ms with an initial 1D structure. In contrast to the moderate gradient regime, these structures *rapidly* undergo decay due to transverse modulations, which leads to the formation of columnar 2D vortex lines [Figures 4(b) and 4(d)], exhibiting a  $2\pi$  phase winding around their core [Fig. 4(f)], and a uniform structure along the direction of view. The numerics also show vortex lines oriented along the orthogonal, horizontal radial axis. In analogy to the scalar case [10], we interpret this behavior as a transverse instability that depends on the relative speeds of the two components, their densities, and the transverse confinement strength.

Dark-dark solitons can also be observed in other settings, e.g., during the mixing of two initially phase-separated components. An experimental result is showcased in Fig. 5. We start from the phase-separated situation in Figs. 5(a) and 5(c) which forms after initially overlapped components experience an axial gradient for 10 s. When the axial gradient is suddenly switched off, the two components interpenetrate, first forming a smooth and extended overlapped region. After some evolution time, individual dark-dark solitons appear [Figs. 5(b) and 5(d)] exhibiting an approximately constant total density (upper blue or dark gray curve). This behavior

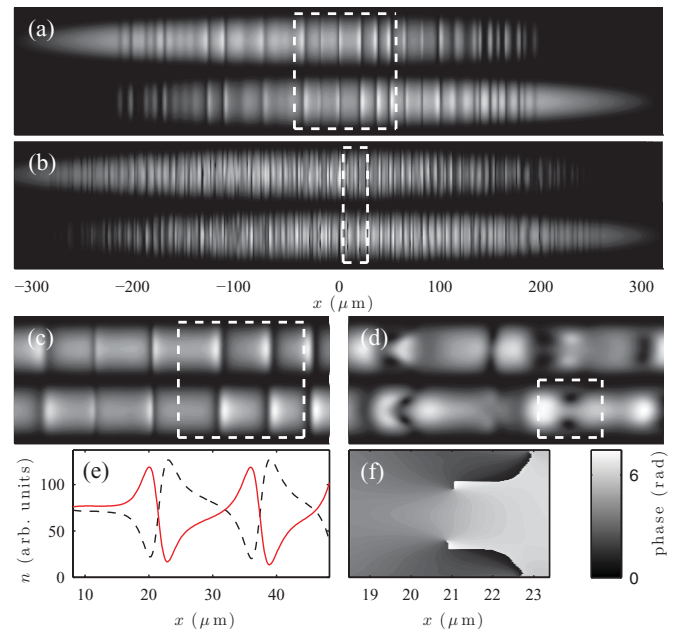


FIG. 4. (Color online) Integrated densities from 3D numerical simulations. (a), (c), (e) correspond to Figs. 3(a) and 3(b) at  $t = 421$  ms with enlargement (c) and line plot (e) of dark-dark solitons. (b), (d), (f) correspond to Figs. 1(a)–1(c) at  $t = 133$  ms with enlargement (d) and a phase plot along the vertical  $z = 0$  plane (f) showing two vortex lines with oppositely oriented  $2\pi$  phase winding. The vertical axes of (a)–(d) span  $16.7 \mu\text{m}$  incorporating a vertical offset of  $8 \mu\text{m}$  between the clouds.

is reminiscent of dark soliton formation in colliding single-component BECs [20]. Beating dark-dark solitons are also theoretically predicted to develop when a repulsive beam is swept through a two-component miscible BEC with an appropriate speed [21].

The beating solitons can be understood through the following simplified model: Assuming that all scattering lengths are equal to  $a_{22}$ , the mean-field equation is the repulsive, vector nonlinear Schrödinger (NLS) equation. Its most general known soliton solution is the six-parameter dark-dark soliton [7] (e.g., two background densities  $n_{1,2}$ , two background flow speeds  $c_{1,2}$ , soliton speed  $v$ , and beating frequency  $\omega$ ) of which the well-studied five-parameter static dark-dark soliton [8] is a

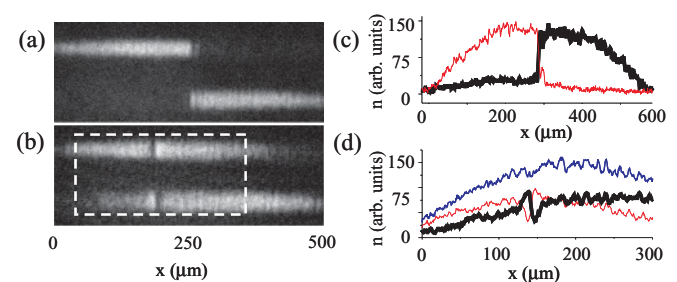


FIG. 5. (Color online) Dark-dark solitons as a result of two-component mixing. (a) Phase-separated mixture in the presence of an axial gradient. (b) Dark-dark soliton formed 1 s after sudden turnoff of the gradient. (c), (d) Integrated cross sections with thin red or light gray (thick black) curve showing the  $|2, -2\rangle$  ( $|1, -1\rangle$ ) component. Blue or dark gray (upper) curve in (d) shows total density.

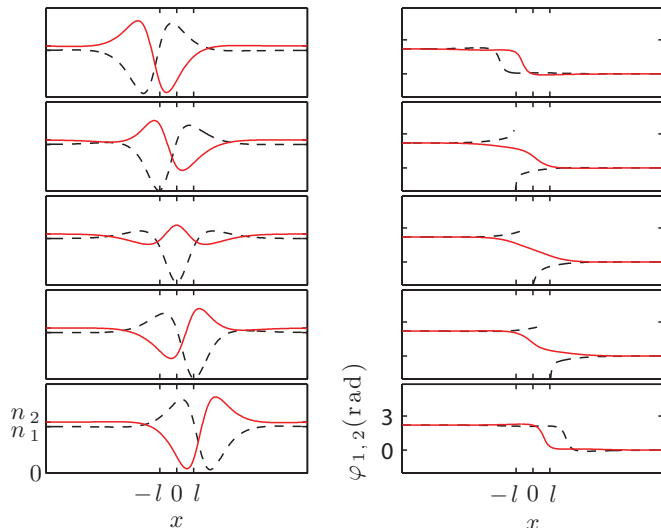


FIG. 6. (Color online) Density and phase evolution of a beating dark-dark soliton assuming equal scattering lengths.

special case. Even though analytical expressions for these solitons were derived [7], their form is quite complicated and basic properties such as the beating frequency as a function of soliton parameters are unknown.

An example of a beating dark-dark soliton can be constructed by leveraging the SU(2) invariance of the vector

NLS equation [15]. Applying a rotation matrix to the two components of a four-parameter dark-bright soliton [8], we obtain a five-parameter beating dark-dark soliton where the background flow speeds are equal to  $c$ . Its evolution over half a beating period is shown in Fig. 6 [compare with Figs. 3(d), 3(e), and 4(e)]. The beating angular frequency  $\omega = \frac{m}{2\hbar}(c-v)^2 \sec^2(\phi/2)$  satisfies [15]

$$m(c-v)^2/(2\hbar) < \omega < \pi\hbar a_{22}(n_1+n_2)/m. \quad (1)$$

The soliton half-width is  $l = \hbar/\sqrt{2m\omega\hbar - m^2(c-v)^2}$ , where  $\phi$  is the soliton phase jump and  $m$  is the particle mass. As  $\omega$  approaches the lower (upper) bound in (1), the beating soliton degenerates to a plane wave (static dark-dark soliton). The beating soliton strongly resembles features observed in experiment and numerical simulations. The predicted minimum oscillation period of 5 ms for our experimental parameters is consistent with the numerically observed periods of  $\sim 15$  ms.

In conclusion, we have presented an experimental observation of a beating dark-dark soliton. These solitons naturally arise from a fast counterflow-induced modulational instability and can emerge during the mixing of two superfluids. Our work opens the door to a range of studies of vector soliton dynamics, with consequences for a diversity of nonlinear, dispersive systems.

P.E. acknowledges support from NSF and ARO. M.A.H. acknowledges support from NSF DMS1008973.

- [1] F. Dalfovo, S. Giorgini, L. P. Pitaevskii, and S. Stringari, *Rev. Mod. Phys.* **71**, 463 (1999).
- [2] P. G. Kevrekidis, D. Frantzeskakis, and R. Carretero-Gonzalez, *Emergent Nonlinear Phenomena in Bose-Einstein Condensates* (Springer, Berlin, 2009).
- [3] V. Zakharov and L. Ostrovsky, *Physica D* **238**, 540 (2009).
- [4] T. B. Benjamin and K. Hasselmann, *Proc. R. Soc. London Ser. A* **299**, 59 (1967).
- [5] V. I. Bespalov and V. I. Talanov, *JETP Lett.* **3**, 307 (1966); A. Hasegawa and Y. Kodama, *Solitons in Optical Communications* (Clarendon, Oxford, UK, 1995).
- [6] P. G. Kevrekidis and D. J. Frantzeskakis, *Mod. Phys. Lett. B* **18**, 173 (2004).
- [7] Q-Han Park and H. J. Shin, *Phys. Rev. E* **61**, 3093 (2000).
- [8] A. P. Sheppard and Y. S. Kivshar, *Phys. Rev. E* **55**, 4773 (1997).
- [9] C. Hamner, J. J. Chang, P. Engels, and M. A. Hofer, *Phys. Rev. Lett.* **106**, 065302 (2011).
- [10] J. Brand and W. P. Reinhardt, *Phys. Rev. A* **65**, 043612 (2002); S. Komineas and N. Papanicolaou, *ibid.* **68**, 043617 (2003).
- [11] The scattering lengths for  $(1, -1)$ ,  $(2, -2)$ , and the interspecies scattering length are approximately  $a_{11} = 100.40$  a.u. and  $a_{22} \approx a_{12} = 98.98$  a.u., respectively [22].
- [12] E. Timmermans, *Phys. Rev. Lett.* **81**, 5718 (1998); P. Ao and S. T. Chui, *Phys. Rev. A* **58**, 4836 (1998); H. Pu and N. P. Bigelow, *Phys. Rev. Lett.* **80**, 1130 (1998).
- [13] C. K. Law, C. M. Chan, P. T. Leung, and M.-C. Chu, *Phys. Rev. A* **63**, 063612 (2001).
- [14] H. Takeuchi, S. Ishino, and M. Tsubota, *Phys. Rev. Lett.* **105**, 205301 (2010).
- [15] See Supplemental Material at <http://link.aps.org/supplement/10.1103/PhysRevA.84.041605> for a description and movies of the numerical simulations, the beating dark-dark soliton solution, and the sound speeds associated with Fig. 2.
- [16] For comparison, the central speed of sound in a single-component BEC with the same total atom number is  $\sim 1.6$  mm/s.
- [17] B. Anderson *et al.*, *Phys. Rev. Lett.* **86**, 2926 (2001).
- [18] C. Becker *et al.*, *Nat. Phys.* **4**, 496 (2008).
- [19] Even though our BEC is elongated, the ratio  $\mu/(\hbar\omega_z) = 6.1$  (where  $\mu$  is the chemical potential and  $\omega_z$  the tightest trapping frequency) puts it into the 3D regime.
- [20] T. F. Scott, R. J. Ballagh, and K. Burnett, *J. Phys. B* **31**, L329 (1998).
- [21] H. Susanto *et al.*, *Phys. Rev. A* **75**, 055601 (2007).
- [22] B. J. Verhaar, E. G. M. van Kempen, and S. J. J. M. F. Kokkelmans, *Phys. Rev. A* **79**, 032711 (2009); S. J. J. M. F. Kokkelmans (private communication).